Theoretical interpretation of W soft X-ray spectra collected by the pulse height analysis system on Wendelstein 7-X stellarator

Special Collection: Proceedings of PLASMA 2023 - International Conference on Research and Applications of Plasmas

Ł. Syrocki ✉ (iD) ; M. Kubkowska (iD) ; S. Jabłoński (iD) ; U. Neuner; W7-X Team

Check for updates

View Online   Export Citation

12 June 2024 10:44:11

Theoretical interpretation of W soft X-ray spectra collected by the pulse height analysis system on Wendelstein 7-X stellarator

View Online   Export Citation   CrossMark

Ł. Syrocki,[1,a)] (iD) M. Kubkowska,[1] (iD) S. Jabłoński,[1] (iD) U. Neuner,[2] and W7-X Team[b)]

AFFILIATIONS

[1]Institute of Plasma Physics and Laser Microfusion, Hery 23, 01-497 Warsaw, Poland
[2]Max Planck Institute for Plasma Physics, 17491 Greifswald, Germany

Note: This paper is part of the Special Topic, Proceedings of PLASMA 2023 - International Conference on Research and Applications of Plasmas.
[a)]Author to whom correspondence should be addressed: lukasz.syrocki@ifpilm.pl
[b)]See Sunn Pedersen *et al.* 2022 (https://iopscience.iop.org/article/10.1088/1741-4326/ac2cf5) for the W7-X Team.

ABSTRACT

In many fusion devices, such as tokamaks or stellarators like Wendelstein 7-X (W7-X), soft x-ray pulse height analysis (PHA) system diagnostics are routinely used during the experiments. The PHA system is dedicated to providing information about the impurity content, and average along line-of-sight electron temperature in the plasma conditions. Moreover, it is also able to estimate impurity density and an average effective charge from the comparison of experimental spectra with the modeled ones. However, the experimental x-ray spectra can be interpreted in terms of interesting plasma parameters only when the theoretical radiation models first identify and then take into account all the relevant factors that affect the spectrum. Therefore, for this purpose, a theoretical model has been applied. Flexible Atomic Code, which allows for calculation of various atomic properties such as energy levels, cross sections for excitation and ionization by electron impact, transition probabilities for radiative transitions and autoionization, and any others as needed in the collisional–radiative approximation. The chosen spectra collected during the W7-X campaign (OP1.2b) were examined, trying to obtain an agreement between the observed and simulated spectra. The analysis carried out allowed for a reliable interpretation of experimental x-ray spectra, estimation of the electron temperature, and obtaining information on the content of tungsten impurities.

I. INTRODUCTION

The development of technology that uses energy released as a result of a controlled thermonuclear fusion of hydrogen isotopes: deuterium and tritium, will be of particular importance for ensuring an efficient and safe source of energy in the future for humans and the environment. This synthesis is being carried out in tokamaks and stellarators and is planned for the ITER reactor ("the way" in Latin).[1]

For some time, in the Wendelstein 7-X (W7-X)[2,3] the world's largest superconducting stellarator in Greifswald, Germany, and in the currently under construction ITER tokamak, heavy metals including tungsten ($Z = 74$) are planned to be used as a material for the construction of their elements (e.g., divertors).[4] Plasma's interaction with the elements of the reactor's chamber wall leads to the release of slight amounts of impurities, passing into the central plasma region, where their characteristic x-ray spectral lines are emitted. The emission of radiation coming from the plasma gives information about the present components and can be used as a diagnostic tool, allowing precise information on key plasma parameters, such as plasma temperature and density, and the content of impurities.[5–12] Therefore, there was an urgent need to develop a precise method of plasma parameters diagnostics, using registered structures of x-ray emission coming from the impurities,[13–20] to provide the optimal conditions for obtaining energy from controlled nuclear fusion.

In this paper, the theoretical model applied, Flexible Atomic Code (FAC),[21] allows for the calculation of various atomic properties such as energy levels, cross sections for excitation and ionization by electron impact, transition probabilities for radiative transitions and

12 June 2024 10:44:11

autoionization, and any others as needed in the collisional–radiative (CR) approximation.

The chosen spectra collected during the W7-X experimental session during the OP1.2b campaign were examined to enable a reliable interpretation and to obtain the agreement between the observed and simulated ones, which allowed to determine the plasma impurities content.

II. EXPERIMENTAL SETUP

The soft x-ray pulse height analysis (PHA) system[22–27] is a standard diagnostic tool used in a wide variety of fusion experiments, allowing the identification of line radiation from relevant contaminants and determining their concentration in the hot plasma core. In general, the temperature averaged, along the line of sight, can be determined using the radiation slope of the hydrogen and low-Z continuum. Moreover, the non-thermal components of the electron distribution can be inferred from the high-energy tail of the recorded spectra. The PHA system was installed on the AEK50 horizontal port on the W7-X in June 2015 (see Fig. 1).

The spectral distribution of energy along the central line of sight is provided by the PHA system diagnostics. The energy resolution is guaranteed to be not worse than 200 eV.

The W7-X system has three energy channels, each with a silicon drift detector (SDD) produced by PNDetector. The nominal energy resolution provided by the manufacturer is 132 eV@5.9 keV (Mn $K\alpha$ line) at an operating temperature of −20 °C. The counting speed is 10 kcps. Zr with an internal diameter of 3.2 mm was used as the collimator. The detectors are equipped with integrated field-effect transistor that improves energy resolution. Measurements are made along the lines of sight passing through the main magnetic axis of the plasma.

Each detector can register the x-ray spectrum in three different energy ranges by selecting one of three beryllium foils of different thicknesses (first channel: open, 10, 25 μm; second channel: open, 50, 100 μm; third channel: 25, 100, 500 μm). This enables the detector's dynamic range to be adjusted to the soft x-ray flux registered for a given wavelength associated with a given impurity species and the

examination of suprathermal tails in the spectra. The first channel is equipped with the SD3 detector with a thin polymer window and aluminum shield, covering the energy range from about 250 eV to 20 keV. The second and third channels are equipped with the standard SDD with a Be window of 8 μm in diameter. The additional filter enables the recording of spectra from 0.9 to 20 and 1.5 to 20 keV, respectively.

For each energy channel, the size of its individual pinhole is controlled to increase or decrease the number of photons reaching the detectors. Each detector can see almost the same volumes of plasma along a line of sight through the center of the plasma with a radial extension of up to 10 cm. Figure 2 shows the PHA system concept with details of the main vacuum chamber. The detectors are mounted on a specially designed vacuum flange ensuring appropriate conditions for heat conduction and electrical insulation. Energy calibration of the recorded spectra is performed by measuring the fluorescence spectra of well-known materials such as Fe, Cu, and Cr.

III. THEORETICAL METHODS—FLEXIBLE ATOMIC CODE

Modeling of the complex structures of the radiation spectrum for highly ionized tungsten present in the plasma was carried out as part of the CR model, using the FAC calculation package.

Modeling emission spectra using the FAC package was performed in two steps:

(a) The first was to determine atomic data such as energy levels, probabilities of radiative and non-radiative transitions, cross sections for various processes (collision excitations, collision ionizations, photoionization), and inverse processes (i.e. radiative and non-radiative capture).

(b) In the second step, having the atomic data obtained (in the first step) and using the CR model, detailed shapes of the characteristic X-ray spectra of elements emitted from the plasma of a given temperature and electron density could be obtained.

The FAC package uses the relativistic Dirac–Fock–Slater (DFS) and the configuration interaction methods to calculate atomic structure parameters (step 1). In short, to determine the energy levels of an atomic ion with N electrons, one needs to perform diagonalization of
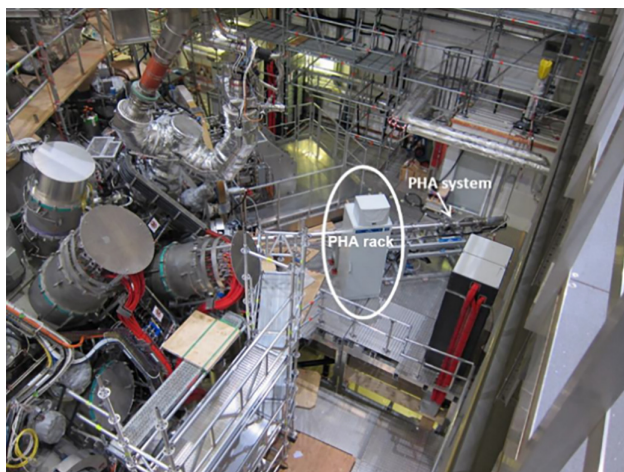

FIG. 1. The PHA system installed on the horizontal port AEK50 of the W7-X.
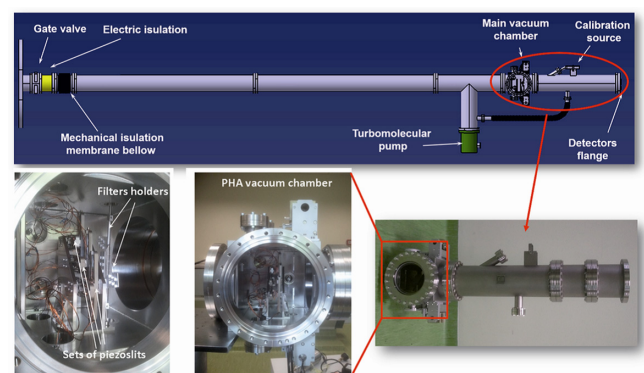

FIG. 2. PHA system for W7-X (top) scheme with details of the main vacuum chamber, which includes piezo-slits and filters (below).

the relativistic effective Hamiltonian H. In atomic units, it looks as follows:

$$\widehat{H} = \sum_{i=1}^{N} h_D(i) + \sum_{j>i=1}^{N} \frac{1}{r_{ij}}, \qquad (1)$$

where the first term in the equation represents the single-electron Dirac Hamiltonian $h_D(i)$ for the potential caused by the nuclear charge. The second term takes into account the interactions between the electrons, where r_{ij} denotes the distance between the ith and jth electrons.

The wave function for the N-electron system (determined by quantum numbers characterizing the total angular momentum J, projection of the angular momentum M, and parity p) is assumed in the form

$$\Psi_s(JM^p) = \sum_m c_m(s)\Phi(\gamma_m JM^p), \qquad (2)$$

where N-electron configuration state functions (CSF) are represented by $\Phi(\gamma_m JM^p)$, and γ_m contains all the information required to uniquely define a certain CSF. The configuration mixing coefficients for state s are denoted by $c_m(s)$ in the same equation. Functions $\Phi(\gamma_m JM^p)$ are presented in the form of a Slater determinant or a combination of Slater determinants built of Dirac single-electron spinors.

The thermodynamic state and population distribution of particular atomic levels in plasma can be described by the CR model, which is the most general plasma model (step 2).

IV. RESULTS AND DISCUSSION
A. 20180809.013 discharge

As can be seen in Fig. 3, after W injection by the Laser Blow-Off (LBO) system[28] and, what is more visible, after W injection by Tracer-Encapsulated Solid Pellet (TESPEL),[29] very interesting peaks at about 8.5 and 10.0 keV appeared in the spectrum observed by the PHA system, during 20180809.013 discharge at W7-X. To perform a reliable interpretation and obtain information about the tungsten impurity content, a simulation using the FAC package was performed for the
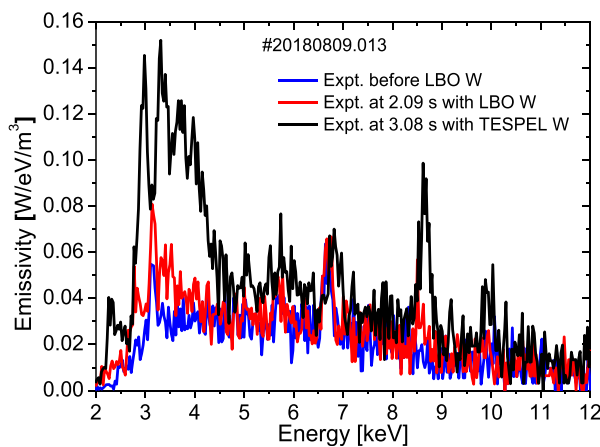
mentioned discharge. For all presented theoretical spectra, the Gaussian function as the instrumental response was assumed.

The results registered after LBO and TESPEL injections are presented in Figs. 3–5, but the detailed analysis is given only for the case with TESPEL injection.

Fractional abundances (FA) of tungsten ions from W^{+23} to W^{+53} in percent were presented in Fig. 6. Calculations were done along the plasma radius for plasma electron temperature achieved during 20180809.013 discharge. The ionic composition for all kinds of tungsten ions has been calculated by solving a set of kinetic equations with the assumption of the coronal plasma model and negligible tungsten radial transport.

Figure 7 presents initial simulations of L x-ray lines of tungsten ions from W^{+47} to W^{+53} taking into account FA (see Figs. 6 and 8), together with the experimental spectrum (20180809.013 discharge) registered at W7-X. The calculation was performed in the range of photon energy from about 7.2 up to 11.0 keV, using the FAC package in the framework of the CR model. This calculation assumed the following electron temperatures: $T_e = 3.5$, 4.5, and 6.0 keV, and single electron density $n_e = 2.5 \times 10^{19}$ m^{-3}. As can be observed, when the electron temperature is relatively low (3.5 keV), the lower ionized tungsten ions W^{+47} and W^{+48} are most dominant. Moreover, the theoretical spectrum is shifted toward lower energies, which may suggest a higher experimental plasma temperature. When the electron temperature starts to increase (4.5 keV), the emissivity of individual ions is significantly different, and what is more, W^{+49}, W^{+48}, and W^{+50} ions start to dominate. In addition, the theoretical spectrum begins to shift toward the experimental spectrum, suggesting an experimental electron temperature of about 5.5 keV. In the case of simulations performed for $T_e = 6$ keV, the largest contribution to the theoretical spectrum comes from the W^{+52} ion. As can be seen, in this case, the theoretical spectrum begins to shift toward higher energies, suggesting that $T_e = 6$ keV is too high in relation to the experimental electron temperature.

The figure presented below shows the FA of tungsten ions in percent, limited to ionization stages from W^{+47} to W^{+53}, which have the biggest influence in the photon energy region between 7.2 and 11 keV. Calculations were done along the plasma radius for plasma electron temperatures achieved during 20180809.013 discharge. As can be seen in Fig. 8, the biggest contribution comes from W^{+51} ion. Figure 9
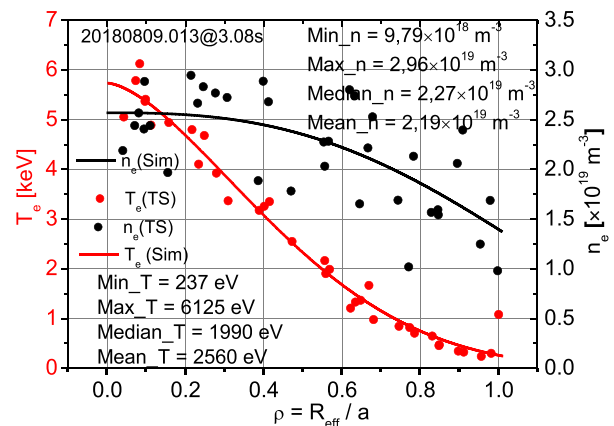
FIG. 3. The PHA spectra in the linear scale without and with injected tungsten impurity for the 20180809.013 W7-X discharge.

FIG. 4. The electron temperature T_e and electron density n_e along the plasma radius together with fitted curves for the 20180809.013 W7-X discharge.
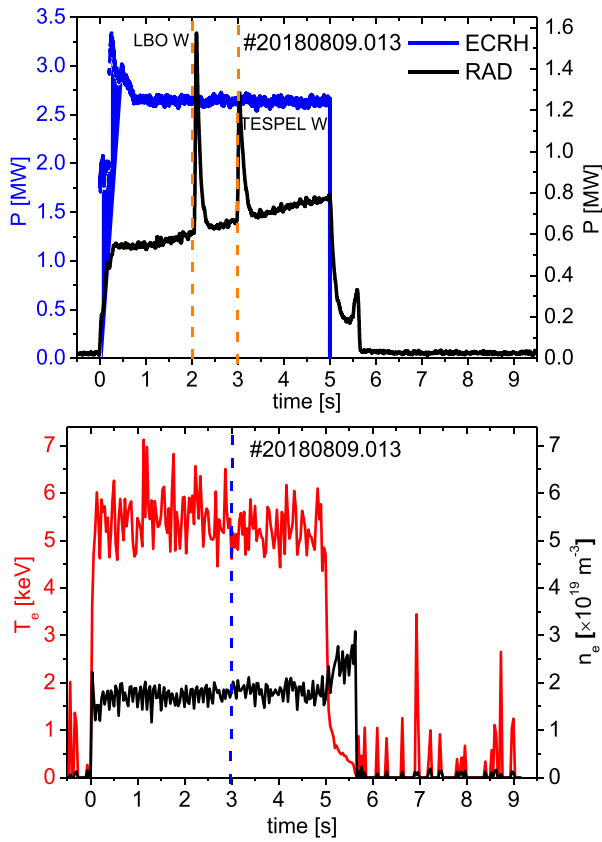
FIG. 5. Time traces of ECRH and radiated power (RAD) with LBO and TESPEL injection of tungsten at 2.0 and 3.0 s, respectively (upper graph), together with time traces of central electron temperature T_e and electron density n_e (lower graph), for the 20180809.013 W7-X discharge.

presents the next step simulation of L x-ray lines of W^{+51} ion, together with the experimental spectrum (20180809.013 discharge) registered at W7-X.

During the simulation, experimental temperature and density profiles obtained by the Thomson scattering (TS) diagnostic and FA of W^{+51} ion were taken into account. Moreover, bremsstrahlung and
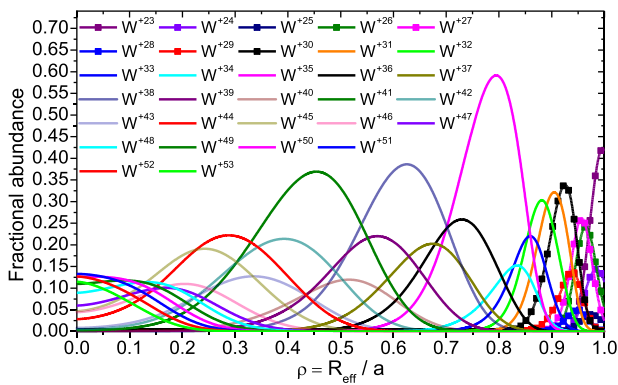

FIG. 6. FA of tungsten ions from W^{+23} to W^{+53} in percent along the plasma radius.
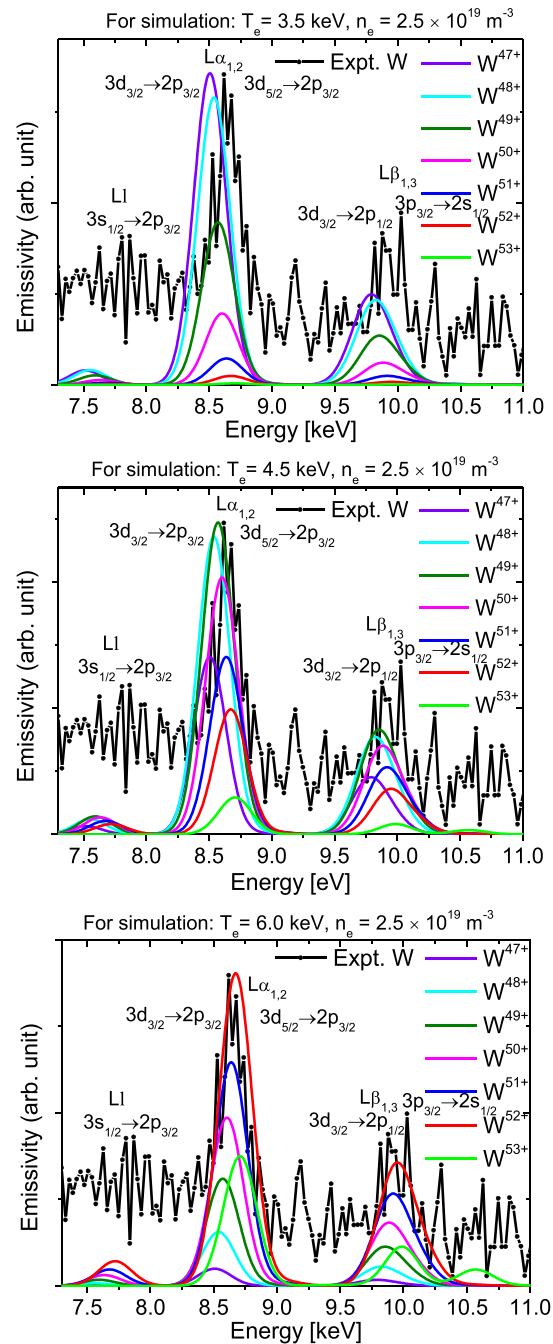

FIG. 7. Simulated L x-ray lines of tungsten ions from W^{+47} to W^{+53} for electron temperatures: $T_e = 3.5$, 4.5, and 6.0 keV, and single electron density $n_e = 2.5 \times 10^{19}$ m^{-3}, using FAC package in the framework of CR model, together with experimental spectrum (20180809.013 discharge) registered at W7-X.

recombination radiation were also included in the simulation to better reflect real plasma conditions. As can be seen, the peak centers of the W^{+51} ion have the same energy as the peak centers in the experimental spectrum.
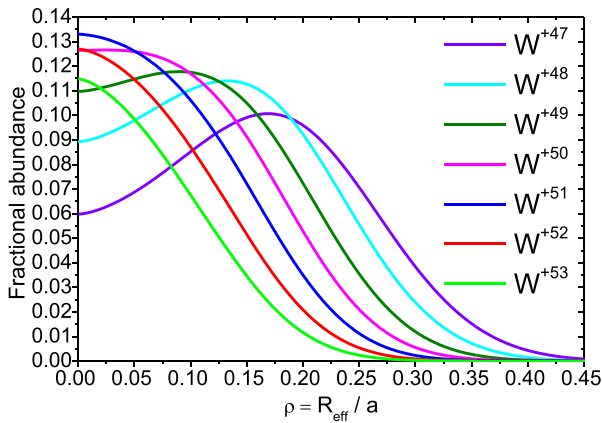
FIG. 8. FA of W in percent along the plasma radius, limited to that ionization stage of W, which has the biggest influence on the spectra.

FIG. 10. Simulated L x-ray lines of tungsten from W^{+47} to W^{+53} ions, background, and summarized spectrum, taking into account experimental T_e and n_e profiles obtained by the TS diagnostic and FA of tungsten, together with experimental spectrum (20180809.013 discharge).

Figure 10 presents the final spectrum obtained during the simulation. In this case, exactly the same simulation procedure was performed as in Fig. 9, but for all ionization stages of tungsten ions that have the biggest influence in the studied region (from W^{+47} to W^{+53}). The contributions of the individual degrees of tungsten ionization in the total spectrum were obtained, which were as follows: 4.38% of W^{+47}, 9.94% of W^{+48}, 14.99% of W^{+49}, 18.68% of W^{+50}, 20.68% of W^{+51}, 23.24% of W^{+52}, and 8.09% of W^{+53}. As can be seen, the theoretical spectrum not only reproduces the experimental spectrum well but also gives the estimation of the tungsten impurity content in the analyzed region of 20180809.013 discharge. Moreover, thanks to the performed analysis, tungsten Ll, $L\alpha_{1,2}$, and $L\beta_{1,3}$ x-ray lines at a photon energy of about 7635, 8625, and 9915 eV, respectively, were identified and observed for the first time at W7-X (see Fig. 10).

B. 20180828.018 discharge

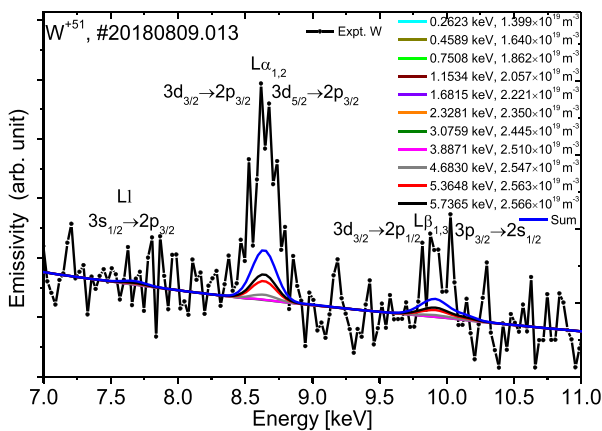Compared to the 20180809.013 discharge, the 20180828.018 discharge (see Fig. 11) has a higher density and lower temperature (see Figs. 12 and 13). This leads to tungsten x-ray lines at lower energies (from 1.5 up to 3.7 keV) than the lines analyzed in Sec. IV A. Therefore, in this case, it was also necessary to conduct simulations in order to interpret the experimental spectrum and obtain reliable information about the content of tungsten impurities. The simulations were done using the FAC package, in the framework of the CR model for experimental conditions shown in Figs. 12 and 13.

During performed analyses, it was found that after taking into account FA (see Fig. 14), bremsstrahlung, and recombination radiation, the lowest energy component centered around 1.65 keV is attributed to the M x-ray lines (transition from the fourth to third shell) mainly in ions from W^{+48} to W^{+44}. The dominant component around 2.1 keV originates from M x-ray lines in tungsten ions from about W^{+30} up to about W^{+50}. In turn, the peaks starting from 2.3 to 3.7 keV also originate from M x-ray lines, but due to $5 \rightarrow 3$ shell transitions excited in W^{+30}–W^{+50} ions. The best match between the results of the simulation and

FIG. 9. Simulated L x-ray lines of W^{+51} ion and background, taking into account experimental T_e and n_e profiles obtained by the TS diagnostic and FA of tungsten, together with experimental spectrum (20180809.013 discharge).
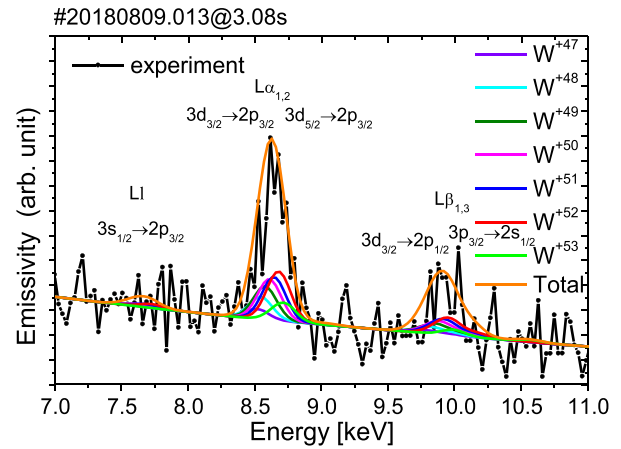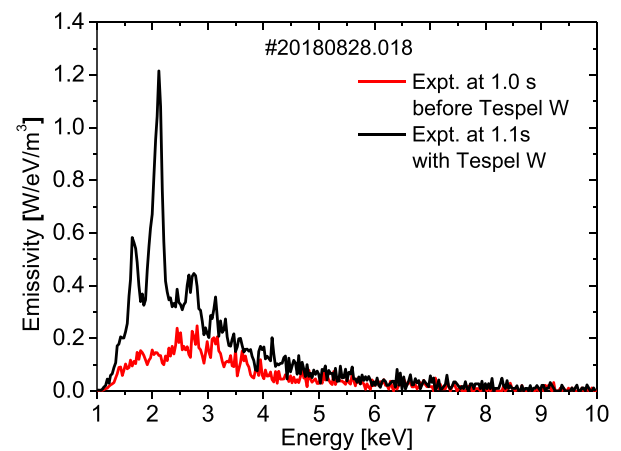

FIG. 11. The PHA spectra in the linear scale without and with injected tungsten impurity at 1.1 s for the 20180828.018 W7-X discharge.
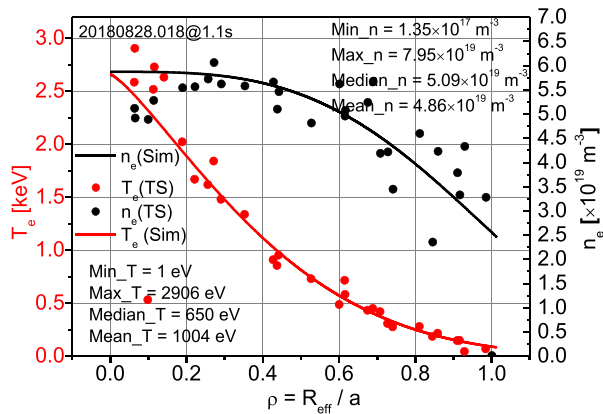
FIG. 12. The T_e and n_e along the plasma radius together with fitted curves for the 20180828.018 W7-X discharge.

the experimental spectrum can be obtained by taking into account tungsten ions in the range from W^{+38} up to W^{+47} (see Fig. 15).

Although the analysis of W x-ray lines around 2.1 keV and from 2.6 up to 3.7 keV showed very good agreement with the experimental
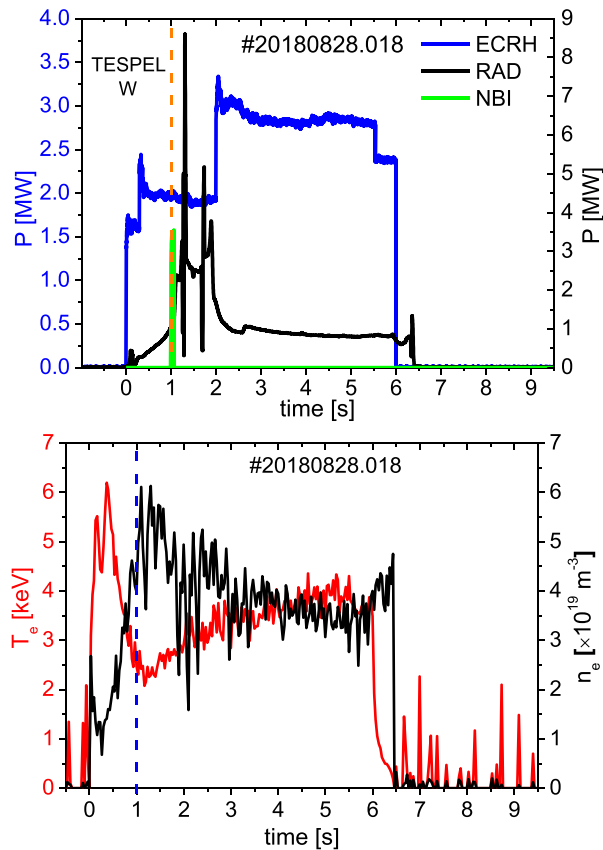

FIG. 13. Time traces of ECRH, RAD, and NBI with TESPEL injection of tungsten at 1.1 s (upper graph), together with time traces of central T_e and n_e (lower graph), for the 20180828.018 W7-X discharge.
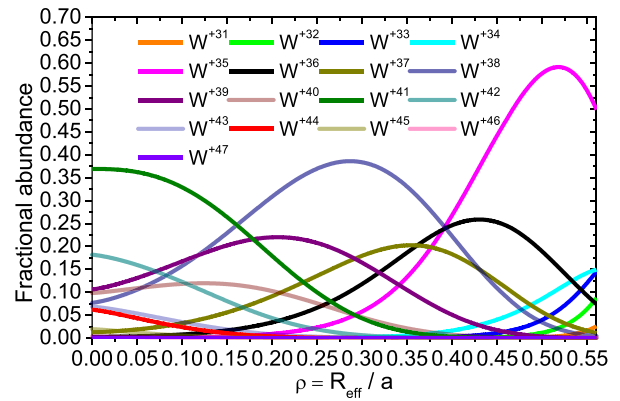

FIG. 14. FA of W in percent along the plasma radius, limited to that ionization stage of W, which has the biggest influence in the photon energy region between 1 and 5 keV.

spectrum, the experimental peak around 1.65 keV is too high in comparison with the result of the simulations. The reason for that seems to be an underestimation of the influence of W^{+44} tungsten ion (see Fig. 16), which probably during the TESPEL W injection, was the most dominant. Therefore, additional experiments and further investigation of the line at around 1.65 keV are needed.

V. CONCLUSIONS

The analysis for 20180809.13 at $t = 3.08$ s and 20180828.18 at $t = 1.1$ s discharges, registered by the PHA system at W7-X during the OP1.2b campaign, was performed. On the base of this analysis, the set of benchmark x-ray spectra for different ionization stages of tungsten, electron temperature, and density of plasma in the energy range of emitted radiation, important for plasma diagnostics on the W7-X stellarator were obtained.
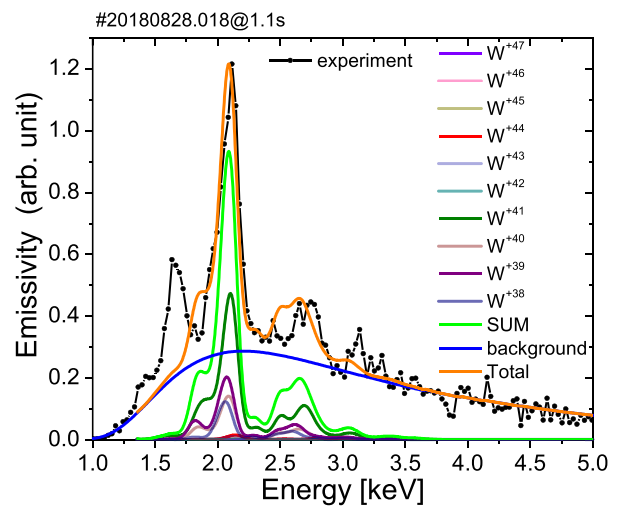

FIG. 15. Simulated x-ray lines of tungsten from W^{+38} to W^{+47} ions, background, and summarized spectrum, taking into account experimental T_e, and n_e profiles obtained by the TS diagnostic, and FA of tungsten ions, together with experimental spectrum (20180828.018 discharge).
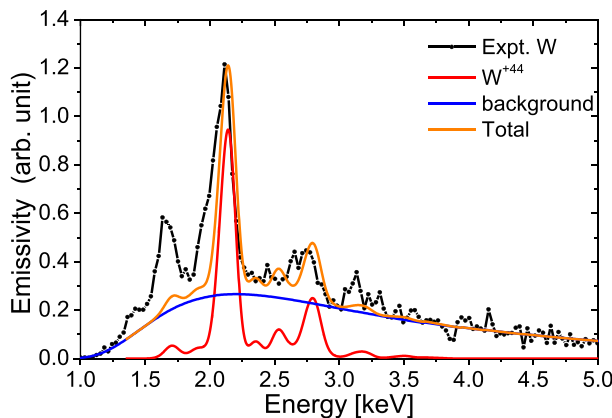
FIG. 16. Simulated x-ray lines of W^{+44} tungsten ion, background, and summarized spectrum, obtained using T_e and n_e from TS diagnostic, and FA of W^{+44}, together with experimental spectrum (20180828.018 discharge).

Thanks to the performed analysis, it was possible to make a reliable interpretation of the experimental x-ray spectra, registered by the PHA system at the W7-X stellarator, estimate electron temperature, and obtain information about the tungsten impurity content. Moreover, the W Ll, $L\alpha_{1,2}$, and $L\beta_{1,3}$ x-ray lines at a photon energy of about 7635, 8625, and 9915 eV, respectively, were identified and observed for the first time at W7-X (see Fig. 10). It was also shown that the FAC code is a tool capable of the simulation of tungsten spectra in plasmas generated at W7-X.

The results of this research may contribute to the development of plasma diagnostics produced at W7-X and the largest tokamak in the world—ITER, currently built (in the south of France).

AUTHOR DECLARATIONS
Conflict of Interest

The authors have no conflicts to disclose.

Author Contributions

Ł. Syrocki: Conceptualization (lead); Data curation (lead); Formal analysis (lead); Investigation (lead); Methodology (lead); Project administration (lead); Resources (lead); Software (lead); Supervision (lead); Validation (lead); Visualization (lead); Writing – original draft (lead); Writing – review & editing (lead). **M. Kubkowska:** Conceptualization (equal); Formal analysis (equal); Investigation (equal); Writing – original draft (equal); Writing – review & editing (equal). **S. Jablonski:** Conceptualization (equal); Formal analysis (equal); Investigation (equal); Writing – original draft (equal); Writing – review & editing (equal). **U. Neuner:** Writing – review & editing (equal).

DATA AVAILABILITY

The data that support the findings of this study are available from the corresponding author upon reasonable request.

REFERENCES

[1]ITER—The way to new energy (2024), https://www.iter.org/.

[2]Wendelstein 7-X (2024), https://www.ipp.mpg.de/w7x.

[3]T. Sunn Pedersen, I. Abramovic, P. Agostinetti, M. Agredano Torres, S. Äkäslompolo, J. Alcuson Belloso, P. Aleynikov, K. Aleynikova, M. Alhashimi, A. Ali et al., "Experimental confirmation of efficient island divertor operation and successful neoclassical transport optimization in Wendelstein 7-X," Nucl. Fusion **62**, 042022 (2022).

[4]J. Fellinger, M. Richou, G. Ehrke, M. Endler, F. Kunkel, D. Naujoks, T. Kremeyer, A. Menzel-Barbara, T. Sieber, J.-F. Lobsien et al., "Tungsten based divertor development for Wendelstein 7-X," Nucl. Mater. Energy **37**, 101506 (2023).

[5]T. Pütterich, R. Neu, R. Dux, A. D. Whiteford, and M. G. O'Mullane, "Modelling of measured tungsten spectra from ASDEX upgrade and predictions for ITER," Plasma Phys. Controlled Fusion **50**, 085016 (2008).

[6]P. Beiersdorfer, J. K. Lepson, M. B. Schneider, and M. P. Bode, "L-shell X-ray emission from neon-like W^{64+}," Phys. Rev. A **86**, 012509 (2012).

[7]Y. Podpaly, J. Clementson, P. Beiersdorfer, J. Williamson, G. V. Brown, and M. F. Gu, "Spectroscopy of $2s_{1/2}-2p_{3/2}$ transitions in W^{65+} through W^{71+}," Phys. Rev. A **80**, 052504 (2009).

[8]P. Beiersdorfer, J. Clementson, J. Dunn, M. F. Gu, K. Morris, Y. Podpaly, E. Wang, M. Bitter, R. Feder, K. W. Hill et al., "The ITER core imaging X-ray spectrometer," J. Phys. B: At. Mol. Opt. Phys. **43**, 144008 (2010).

[9]R. Neu, K. B. Fournier, D. Bolshukhin, and R. Dux, "Spectral lines from highly charged tungsten ions in the soft-x-ray region for quantitative diagnostics of fusion plasmas," Phys. Scr. **T92**, 307 (2001).

[10]J. Clementson, P. Beiersdorfer, E. W. Magee, H. S. McLean, and R. D. Wood, "Tungsten spectroscopy relevant to the diagnostics of ITER divertor plasmas," J. Phys. B: At. Mol. Opt. Phys. **43**, 144009 (2010).

[11]Y. Ralchenko, IN. Draganić, D. Osin, J. D. Gillaspy, and J. Reader, "Spectroscopy of diagnostically important magnetic-dipole lines in highly charged $3d^n$ ions of tungsten," Phys. Rev. A **83**, 032517 (2011).

[12]J. Clementson and P. Beiersdorfer, "Wavelength measurement of n=3 to n=3 transitions in highly charged tungsten ions," Phys. Rev. A **81**, 052509 (2010).

[13]K. Słabkowska, M. Polasik, E. Szymańska, J. Starosta, Ł. Syrocki, J. Rzadkiewicz, and N. R. Pereira, "Modeling of the L and M X-ray line structures for tungsten in high-temperature tokamak plasmas," Phys. Scr. **T161**, 014015 (2014).

[14]K. Słabkowska, J. Rzadkiewicz, Ł. Syrocki, E. Szymańska, A. Shumack, M. Polasik, and N. R. Pereira, and JET Contributors. "On the interpretation of high-resolution X-ray spectra from JET with an ITER-like wall," J. Phys. B: At. Mol. Opt. Phys. **48**, 144028 (2015).

[15]T. Nakano, A. E. Shumack, C. F. Maggi, M. Reinke, K. D. Lawson, I. Coffey, T. Pütterich, S. Brezinsek, B. Lipschultz, G. F. Matthews et al., "Determination of tungsten and molybdenum concentrations from an X-ray range spectrum in JET with the ITER-like wall configuration," J. Phys. B: At. Mol. Opt. Phys. **48**, 124023 (2015).

[16]K. Słabkowska, M. Polasik, Ł. Syrocki, E. Szymańska, J. Rzadkiewicz, and N. R. Pereira, "Modeling of the M X-ray line structures for tungsten and L X-ray line structures for molybdenum," J. Phys: Conf. Ser. **583**, 012036 (2015).

[17]K. Słabkowska, Ł. Syrocki, E. Węder, and M. Polasik, "Individual contributions of M X-ray line from Cu- and Co-like tungsten ions and L X-ray line from Ne-like molybdenum ions—Benchmarks for new approach to determine the high-

temperature tokamak plasma parameters," Nucl. Instrum. Methods B **408**, 265 (2017).

[18] Ł. Syrocki, K. Słabkowska, E. Węder, J. Starosta-Sztuczka, and M. Polasik, "Modeling of soft N, M and L X-ray lines from tungsten relevant to plasma parameters in the WEST tokamak," Nucl. Instr. Meth. Phys. Res. B **408**, 257 (2017).

[19] J. Rzadkiewicz, Y. Yang, K. Kozioł, M. G. O'Mullane, A. Patel, J. Xiao, K. Yao, Y. Shen, D. Lu, R. Hutton, Y. Zou, and JET Contributors. "High-resolution tungsten spectroscopy relevant to the diagnostic of high-temperature tokamak plasmas," Phys. Rev. A **97**, 052501 (2018).

[20] Ł. Syrocki, K. Słabkowska, E. Węder, M. Polasik, and J. Rzadkiewicz, "Theoretical modeling of high-resolution X-ray spectra emitted by tungsten and molybdenum ions from tokamak plasmas," J. Fusion Energy **39**, 194 (2020).

[21] M. F. Gu, "The flexible atomic code," Can. J. Phys. **86**, 675 (2008).

[22] D. Pasini, R. D. Gill, J. Holm, E. van der Goot, and A. Weller, "JET x-ray pulse-height analysis system," Rev. Sci. Instrum. **59**, 693 (1988).

[23] S. Muto and S. Moria LHD Experimental Group. "First result from X-ray pulse height analyzer with radial scanning system for LHD," Rev. Sci. Instrum. **72**, 1206 (2001).

[24] M. Kubkowska, A. Czarnecka, W. Figacz, S. Jabłoński, J. Kaczmarczyk, N. Krawczyk, L. Ryć, C. Biedermann, R. Koenig, H. Thomsen, A. Weller, and W

7-X Team, "Laboratory tests of the pulse height analysis system for Wendelstein 7-X," J. Instrum. **10**, P10016 (2015).

[25] N. Krawczyk, C. Biedermann, A. Czarnecka, T. Fornal, S. Jabłoński, J. Kaczmarczyk, M. Kubkowska, F. Kunkel, K. J. McCarthy, L. Ryć *et al.*, "Commissioning and first operation of the pulse-height analysis diagnostic on Wendelstein 7-X stellarator," Fusion Eng. Des. **123**, 1006 (2017).

[26] Z. Y. Chen, B. N. Wan, Y. J. Shi, L. Q. Hu, S. Y. Lin, Q. S. Hu, and S. X. Lui, "A compact soft X-ray PHA in the HT-7 tokamak," Nucl. Instrum. Methods Phys. Res. A **527**, 604 (2004).

[27] A. Weller, B. Huber, J. Belapure, T. Pütterich, M. Sertoli, A. Gude, R. Neu, R. Dux, and W. Suttrop, "X-ray pulse height analysis on ASDEX upgrade," in *38th EPS Conference on Plasma Physics* (EPS, 2011).

[28] T. Wegner, B. Geiger, F. Kunkel, R. Burhenn, T. Schröder, C. Biedermann, B. Buttenschön, G. Cseh, P. Drews, O. Grulke *et al.*, "Design, capabilities, and first results of the new laser blow-off system on Wendelstein 7-X," Rev. Sci. Instrum. **89**, 073505 (2018).

[29] R. Bussiahn, N. Tamura, K. J. McCarthy, R. Burhenn, H. Hayashi, R. Laube, T. Klinger, and LHD Experiment Group, W7-X Team. "Tracer-Encapsulated Solid Pellet (TESPEL) injection system for Wendelstein 7-X," Rev. Sci. Instrum. **89**, 10K112 (2018).